The Antarctic Slope Current near 30°E

Jun Dong, Kevin Speer, Loïc Jullion

AGU PUBLICATIONS

JGR

Journal of Geophysical Research: Oceans

RESEARCH ARTICLE

10.1002/2015JC011099

The Antarctic Slope Current near 30°E

Jun Dong[1,2], Kevin Speer[1], and Loic Jullion[3]

[1]Department of Earth, Ocean, and Atmospheric Sciences and the Geophysical Fluid Dynamics Institute, Florida State University, Tallahassee, Florida, USA, [2]ESSIC, University of Maryland, College Park, Maryland, USA, [3]Mediterranean Institute of Oceanography Marseille, France

Key Points:
- Antarctic Slope Current transport near 30 E is estimated to be 9.6 ± 2.3 Sv
- The Antarctic Slope Front transport is 4.0 ± 0.3 Sv
- 1.8 ± 0.03 Sv enters the Weddell Gyre as recently formed dense water

Correspondence to:
K. Speer,
kspeer@fsu.edu

Citation:
Dong, J., K. Speer, and L. Jullion (2016), The Antarctic Slope Current near 30°E, *J. Geophys. Res. Oceans*, *121*, 1051–1062, doi:10.1002/2015JC011099.

Received 2 JUL 2015
Accepted 5 JAN 2016
Accepted article online 12 JAN 2016
Published online 1 FEB 2016

Abstract The Antarctic Slope Current flows westward above the continental slope of Antarctica, entering the Weddell Sea near 30°E and supplying dense water to the deep overturning cell there, and contributing to global Antarctic Bottom Water formation. Observations from the 2008 I6S hydrographic section are used to investigate the strength of the Slope Current near 30°E. A prominent topographic feature, the Gunnerus Bank, diverts the Slope Current upstream of this longitude, and has a large effect on the current's structure, splitting it into a coastal and offshore component. The bank also enhances water mass mixing and lateral exchange across the slope. As part of the 2008 occupation, an additional line was made along the crest of the bank, forming a closed volume over the western side. By combining hydrographic and Lowered Acoustic Doppler Current Profiler measurements in this box using an inverse method, the Slope Current transport is estimated to be 9.6 ± 2.3 Sv; the transport associated with the Antarctic Slope Front is 4.0 ± 0.3 Sv, of which 1.8 ± 0.3 Sv enters the Weddell Gyre as recently formed dense water.

1. Introduction

In February–March 2008, the I6S line south of Africa along 30°E to the Antarctic margin was occupied under the auspices of the US Climate Variability (CLIVAR) Repeat Hydrography program. The 2008 I6S section was a nominal repeat of the World Ocean Circulation Experiment (WOCE) section occupied in February–March 1996 by the French WOCE program. Additional observations, forming a boxed region, were made in 2008 at the southern end of the section across the Gunnerus Bank (Figure 1) between latitude 65°S and 68.5°S. The Gunnerus Bank is an extensive submarine ridge extending northward about 260 km from the Antarctic continent, with a typical depth of roughly 1000 m over much of its length. It is about 55 km wide, and the water depth around the Gunnerus Bank increases from 1200 to 4000 m rapidly on three sides. The 2008 I6S occupation provided an opportunity to study the water mass distribution, currents, and transport near this bank and the Antarctic continent.

The Antarctic continental margin is a region where the shallow shelf and deep ocean water masses meet, as isopycnal layers rise toward the surface. The nature of water mass transport and mixing in this region influences both physical and biological processes through heat, salt, chemical and nutrient exchange. The dominant hydrographic feature on the Antarctic margin is the Antarctic Slope Front (ASF) and the associated westward Antarctic Slope Current (ASC) [*Whitworth et al*., 1998]. *Gill* [1973] explained the dynamics of the ASC as a result of the generally westward wind near the continental margin piling the surface water against the coast by Ekman transport, generating via geostrophic balance a westward-moving current.

Moving west along the margin in the Enderby Basin, from the Kerguelen Plateau toward the Weddell Sea, the ASC is, at some point, considered to be part of the Weddell Gyre. The Antarctic continent bounds the Weddell Gyre to the south and west, and the mid-ocean ridge forms the northern limit. *Gill* [1973] placed the eastern boundary of the Weddell Gyre between 20°E and 30°E because of the large southward bend of the ACC. *Park et al*. [2001] argued that the eastern boundary could be placed as far as 60°E based on CFC-12 distribution. *Schroder and Fahrbach* [1999] described the regional circulation not so much as a gyre, but as a decay of the eastward mean flow in the northeast and build-up of westward flow in the south.

Much attention and observational efforts have focused on the southwestern Weddell Gyre because it is the site of bottom water formation and a source of subsequent outflow [*Gill*, 1973; *Whitworth*, 2000; *Klatt et al*., 2005]. However, the eastern region of the Weddell Gyre is important because Antarctic Circumpolar Current

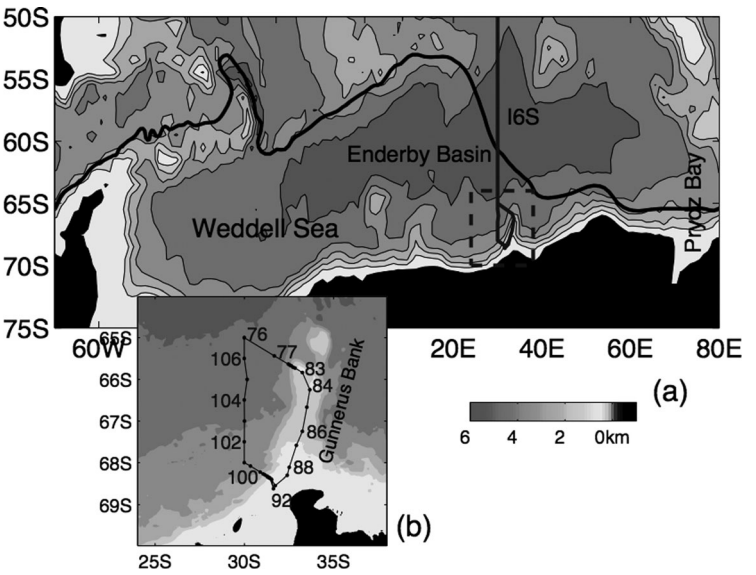

Figure 1. Station locations and bathymetry (from the Smith and Sandwell data set). Inset shows expanded view of stations and Gunnerus Bank. The boundary between the Weddell Gyre and the ACC from *Orsi et al*. [1995] is indicated (black curve) along with the I6S cruise section. The observations described here lie within the box at the southern end of I6S.

(ACC) water masses can mix and exchange properties with the gyre in this region [*Park et al*., 2001; *Klatt et al*., 2005], modifying the heat and salt balance of the gyre. Moreover, on the continental margin, the deep water entering the gyre (typically below 2500 m) contains newly formed water mass products from upstream sources [*Meredith et al*., 2000; *Hoppema et al*., 2001; *Schodlok et al*., 2001]. Recent work by *Jullion et al*. [2014] suggests that this upstream source of dense water is the primary component of bottom water exiting the Weddell Sea.

The I6S section passes through the eastern Weddell Gyre boundary and extends to the shelf, crossing the ASC. Relatively few observations exist in this region compared to areas farther west or east, and the presence of the Gunnerus Bank introduces a dramatic obstacle to the westward flowing Slope Current. Our aim is to examine the effect of the Bank, and to distinguish the circulation near the margin from the interior gyre flow, in order to determine the strength of the Slope Current and the net inflow to the Weddell Gyre.

Flow on the shelf is also a critical component of the circulation. *Hellmer et al*. [2012] have described the potentially dramatic consequences of the Coastal Current, situated farther west, on the Filchner-Ronne ice-shelf mass budget in a warming climate, suggesting that interaction between this current and the ice-shelf could be stronger than in the present climate. The surface stress forcing the current can vary with ice cover, and, in turn, a redirected current may exert control over the ice cover and ice sheet boundary. We show that a Coastal Current also exists near 30°E, on the Gunnerus Bank.

This paper is organized as follows. The I6S cruise data are introduced in section 2 and the distribution of water masses is discussed in section 3. In section 4, the circulation near Gunnerus Bank is investigated by means of a simple inverse model that balances mass, heat, and salt fluxes in isopycnal layers. Based on this model, transport is estimated together with interior diapycnal fluxes. A summary and discussion is provided in section 5.

2. Data

We use observations from the southern part of the 2008 CLIVAR I6S Repeat Hydrography survey, including 31 stations forming a boxed region over the Gunnerus Bank (Figure 1). The stations were occupied clockwise from station 76 to 106, and took 8 days to complete. The station spacing is about one-half degree in the open ocean region and then on every 500 m isobath across the slope. The hydrographic stations were undertaken using a SeaBird CTD with an oxygen sensor mounted on a 36 bottle rosette. The CTD data were processed by the Scripps Ocean Data Facility, with accuracies of 0.001°C for temperature, 0.002 psu for salinity. Oxygen data show post cruise calibrated deep standard deviation which is quite low, about 1 μmol/kg, and the accuracy is expected to be about 2 μmol/kg (for details on oxygen and nutrient calibrations, see *Speer et al*. [2009]). CFC accuracy is ±2%.

A downward-looking Lowered Acoustic Doppler Current Profiler (LADCP; 300 kHz) was mounted on the rosette and directly measured the velocity fields at each of the stations. A shipboard ADCP (SADCP), using 150 kHz frequency, was mounted on the vessel, and continuously recorded and binned the velocity measurement every 5 min for the upper 300 m depth. The data were processed using the Lamont Doherty Earth

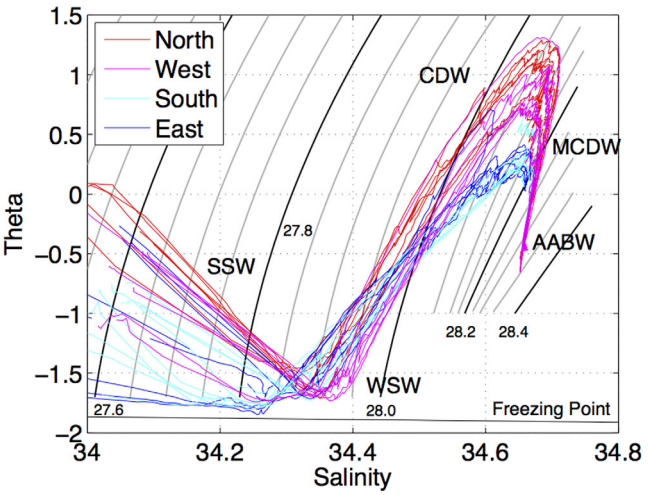

Figure 2. TS diagram of all the box stations. The stations are divided into four sections and the major water masses are labeled. The contour lines are fitted neutral densities from the Southern Ocean Atlas [*Orsi et al.*, 1995].

Observatory (LDEO) software [*Thurnherr*, 2012], which uses an inverse method to get the best estimate of the ocean velocities combining the bottom tracking velocity, SADCP, and other navigation data. In the box region, LADCP data at two stations 80 and 91 were dropped because the inverse method could not get consistent results for these stations. Average LADCP velocity error is ±3.6 cm/s and SADCP error is ±2.6 cm/s.

The "box" comprising the southern end of the I6S observations is roughly divided into four sides (north, south, west, and east). To better present the property distributions, the south and west sections are combined together

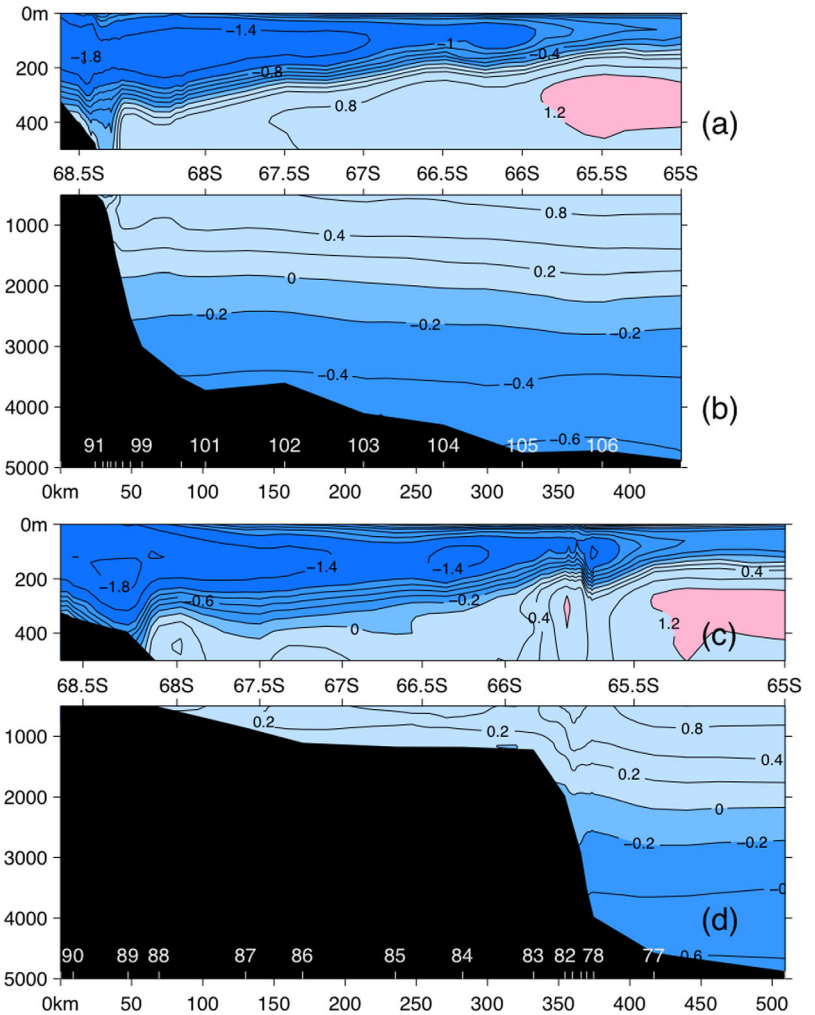

Figure 3. Potential temperature (°C) of the western section (STATIONS 91-106-76; a and b) and the eastern section (STATIONS 76-90; c and d) from CTD data. The upper 500 m in both sections are stretched to show more details (a and c). Selected station numbers are shown at the bottom (b and d).

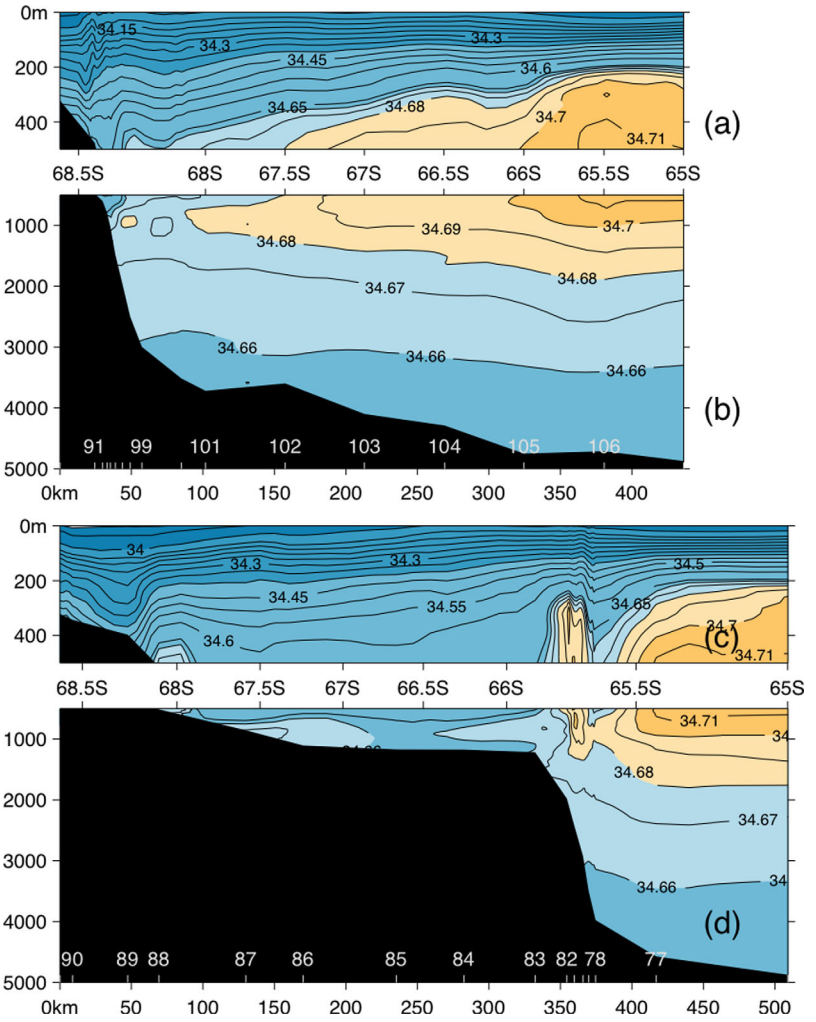

Figure 4. Salinity (psu; CTD data) of the western section and the eastern section as in Figure 3.

as the western section, and the north and east sections are combined together as the eastern section. Property distributions will be described next, documenting the origins of water masses surrounding the Gunnerus Bank, and to place the frontal structures in context, followed by an analysis of the flow and transport estimates.

3. Water Masses

The upper few hundred meters of the water column shows warmer summer surface water and remnant winter surface water, characterized by a temperature minimum near the freezing point and salinity of 34.2–34.4 psu (Figure 2). The temperature minimum deepens from near 50 m offshore to about 150 m depth above the shelf break, then shoals somewhat inshore, remaining stratified by salinity (Figures 3–5). Temperatures and salinities increase with depth, while oxygen concentrations decrease (Figure 6), to extrema associated with the Circumpolar Deep Water (CDW) layer, the upper boundary corresponding to the temperature maximum near 400 m depth at the outer limit of the section. The temperature of this layer above the 3000 m isobath, used by *Whitworth et al*. [1998] to characterize the circumpolar zonal variation of this layer, increases abruptly from about 0.5°C to 1.0°C running eastward along the slope from the western section to the eastern section at the tip of the Gunnerus Bank, representing a large fraction of the total change from the Weddell Sea to the Ross Sea.

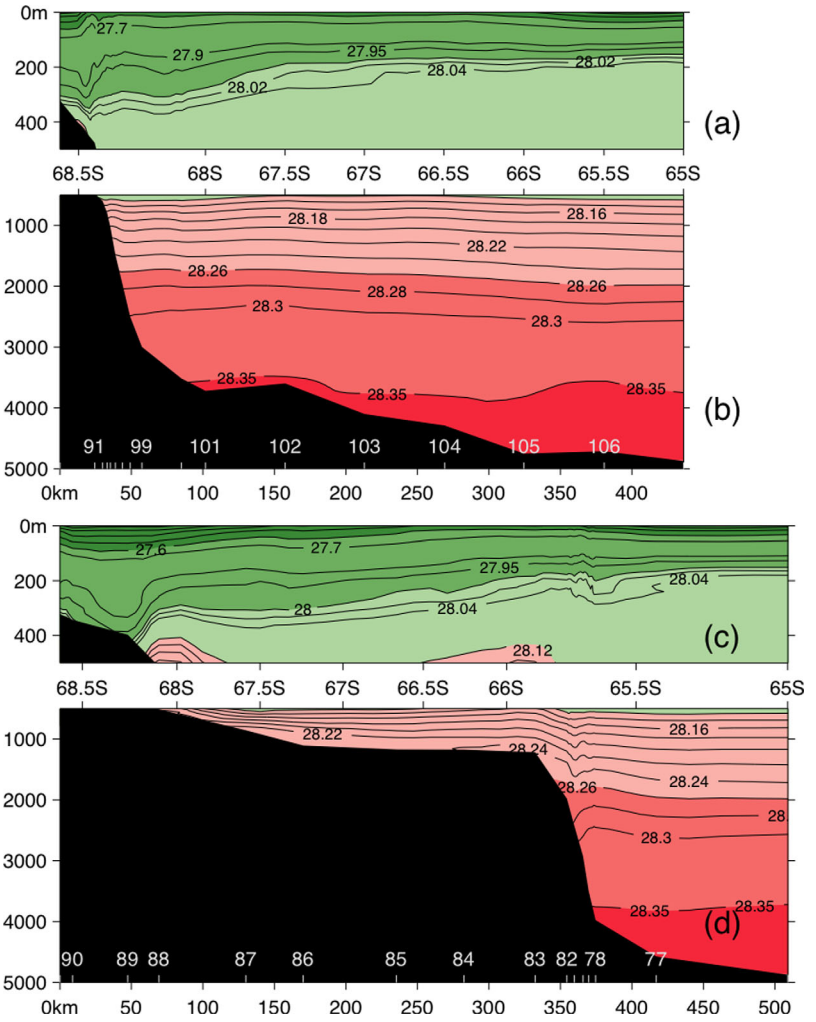

Figure 5. Neutral density (kg/m^3) of the western section and the eastern section as in Figure 3.

The CDW mass is modified by mixing to different degrees, evident on the T-S curve as an eroding temperature maximum over the Gunnerus Bank (the south and east sections, Figure 2; Stations 83–101). At the southern end of the bank the temperature of the maximum has dropped to near 0.2°C, similar to values much farther west in the Weddell Sea, and well within *Whitworth et al.*'s [1998] regional definition of CDW in the Weddell Sea. The mix of CDW with cold, fresh overlying water on the bank also erodes the temperature minimum and shifts it to lower salinity, similar to the cold, inshore wedge of Antarctic Surface Water described by *Heywood et al.* [2000] near 17°W [see also *Carmack*, 1974]. On the southern part of the bank section (Stations 88–92), water at the bottom is relatively salty and warm, but this water can be explained by lateral exchange with the CDW. Unlike regions near large ice sheets in the southwestern Weddell Sea, there is no relatively salty Shelf Water near the freezing temperature with salinities greater than 34.5 psu in this area, hence no indication of the local production of Antarctic Bottom Water.

An Antarctic Slope Front (ASF) and associated Slope Current are evident from the sharp downward sloping isotherms and isopycnals in the western section near the shelf break (Figures 3a and 5a). Below 500 m this slope reverses, suggestive of the eastward undercurrent conditions described by *Chavanne et al.* [2010]. LADCP measurements, discussed in the following section, did show a flow reversal near 500 m depth, but sampling down the slope was inadequate to resolve directly any flow reversal near the bottom at greater depths.

The ASF is split on the Gunnerus Bank (eastern) section with a strong hydrographic front inshore, over the shelf near 68 S, and weaker one offshore, above the slope (Figures 3–5c, 5d near 65.8°S). This differs

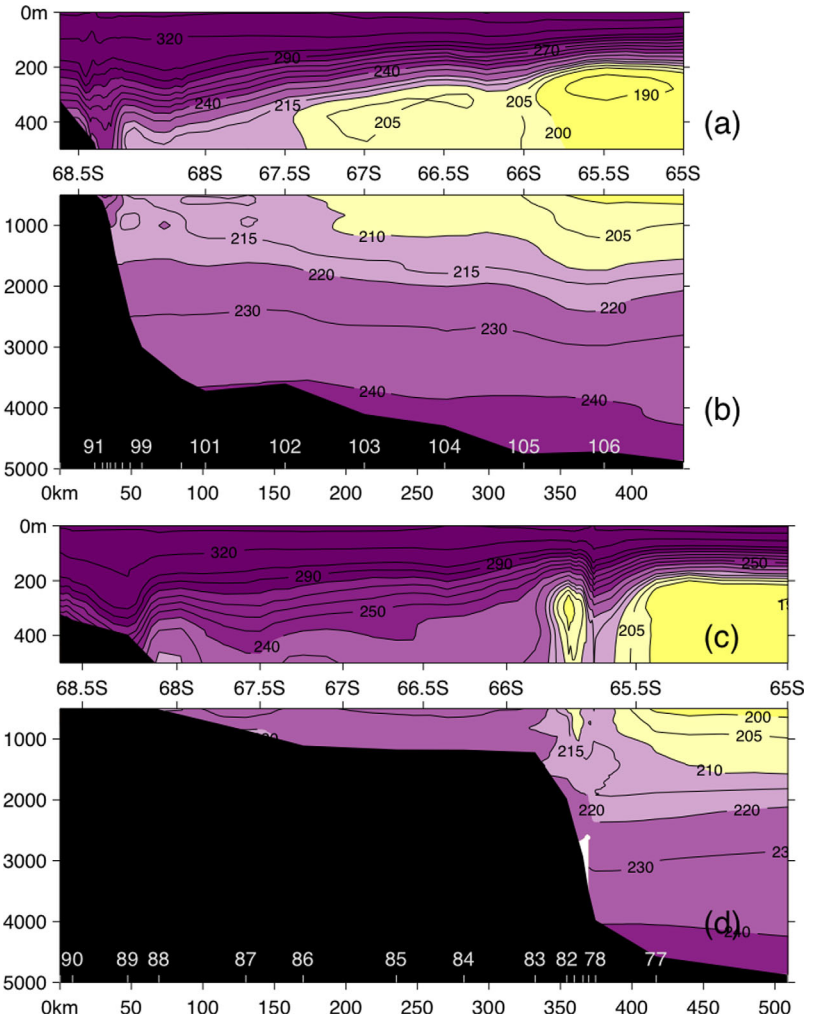

Figure 6. Oxygen (μmol/kg) of the western section and the eastern section as in Figure 3.

somewhat from the map of the distribution of the 0°C contour at 400 m in *Whitworth et al.* [1998] which shows the ASF following the curvature of the bank approximately along isobaths, and they emphasize the association of the Slope Current with the ASF. The outer bank front above the slope (Stations 78–83) is also associated with the terminus of the temperature maximum at the bank; that is, the temperature maximum layer is weak or absent over the bank. Similarly, except for a weak signal near 500 m depth on the bank, the salinity maximum layer ends at the outer bank. The inshore front found here forms, on the shelf, what has farther to the west been called the Coastal Current [see *Heywood et al.*, 2000; *Fahrbach et al.*, 1992]. It merges with the Slope Current on the western side of the bank (Figure 9).

On both the western and eastern sections, the upslope excursion, or shoaling, of isopycnals close to the bottom near 500 m depth brings warmer, saltier water up the shelf (Figures 3–5). This effect appears near the bottom despite the generally oppositely (downward to the south) sloped isopycnals above. At this longitude, the ice-shelf is inshore of the 300 m isobath; farther west the ice-shelf extends out over the shelf to greater depths. The uplift and mixing at the margins of the continental slope near 30°E, associated with the bank, may be responsible for a reduced extension of the shelf. The effects of the penetration of warmer water may also be felt farther downstream, influencing the characteristics of the water under the ice-shelves as well as glacial ice-melt rates.

Our measurements do not allow us to infer the mechanism for isopycnal shoaling. *Chavanne et al.* [2010] associate the isopycnal slope reversals with the approximate thermal wind balance in a transient undercurrent generated by coastally trapped waves. *Nøst et al.* [2011] examine mechanisms for the exchange of

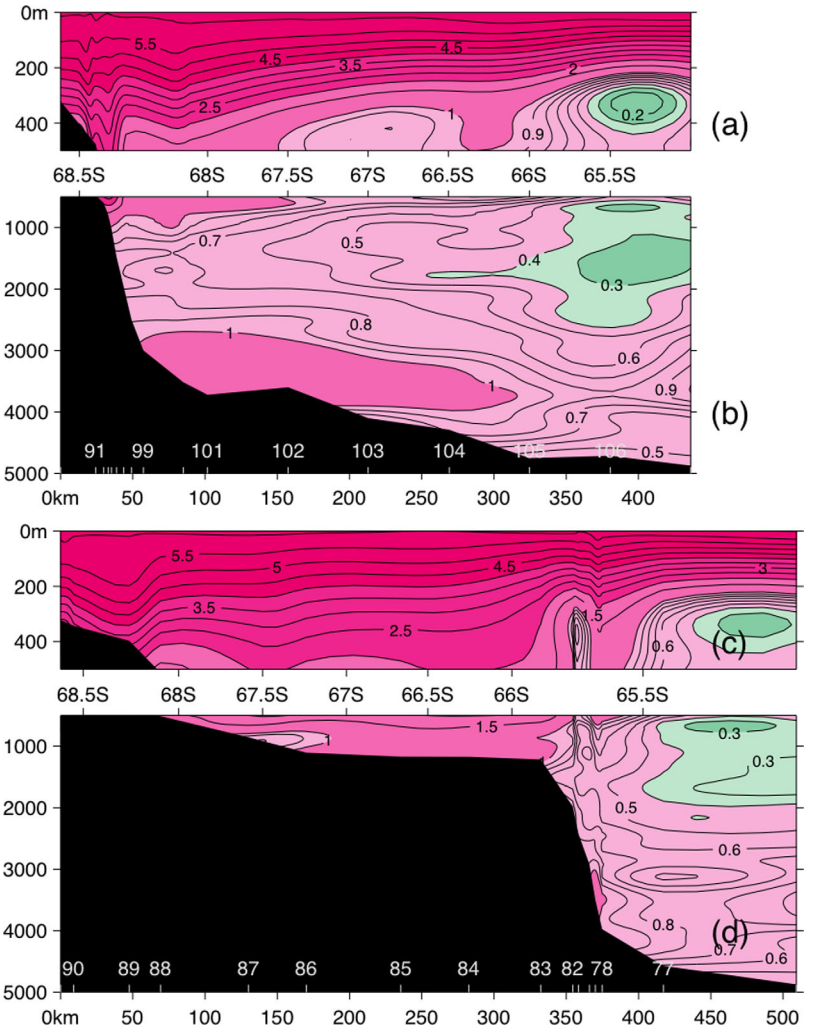

Figure 7. CFC-11 (pmol/kg; from water samples) of the western section and the eastern section as in Figure 3.

water across the ASF in the eastern Weddell Sea and conclude that eddy advection plays an important role in the shoaling of isopycnals near the bottom and the associated onshore transport of WDW. In either case, transient flow creates cross-slope excursions of the density field and an opportunity for mixing to produce a net transfer of WDW properties to the upper shelf.

At the base of the continental slope relatively high CFC concentration was found (Figure 7), lying roughly between 3000 and 4500 m depth. As noted by *Archambeau et al*. [1998], this high CFC is weakly correlated with higher oxygen concentration (Figure 6), suggestive of more recent ventilation. *Couldrey et al* [2013] examined deep water property changes along the southern end of I6S and regionally to determine the origin of these changes, and support the inference that sources near Prydz Bay (see Figure 1) supply new dense water which flows westward along the base of the slope. We mapped the depth of a neutral density layer in the core of the high CFC eastward along the margin using the Southern Ocean Database (not shown); this neutral density layer rises to shelf depths near Prydz Bay.

4. Current and Transport

Direct current measurements with a LADCP and SADCP are used in the following together with hydrographic station data to describe the flow across the sections; then, by combining the current measurements with heat and salt conservation using a simple inverse method, an estimate of the transport is obtained.

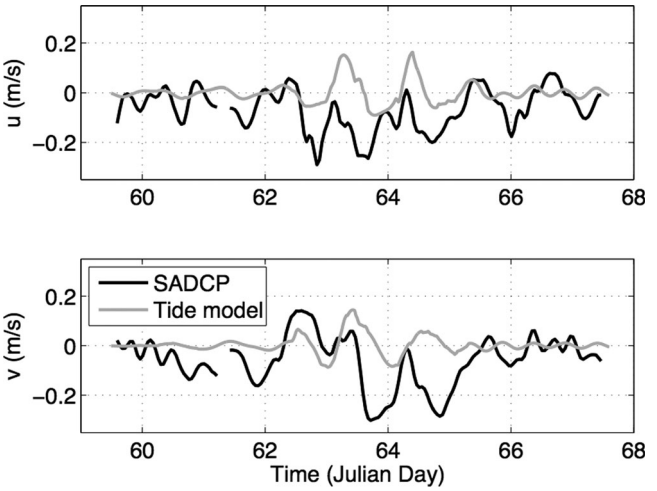

Figure 8. Shipboard ADCP velocities averaged between 100 and 200 m along with tidal velocities for comparison. Time is the Julian Day referenced to 1 January 2008.

4.1. Current Measurements

In shallow water, the tide may have a large effect on the velocity field. Therefore, a tidal component was investigated by comparing the continuous SADCP measurement with a tidal model. The SADCP velocity was averaged between 100 and 200 m to decrease the measurement noise. The tidal model we used is the SER/OSU suite of high-latitude barotropic tide models, CATS02.01. The CATS02.01 model is a forward regional model of the entire circum-Antarctic ocean to 58°S with medium-resolution, 1/4°×1/12° (∼10 km). During days 62 to day 65 (Figure 8; corresponding to stations on the bank), strong tidal components of about 10 cm/s were found, consistent with observations from the SADCP.

The tidal model was also used to remove tidal effects from the LADCP data. After removing the tide, an assessment of the importance of the adjustment was made by calculating mass imbalance in the southern box. The box volume transport imbalance decreased from 20 Sv without detiding to 16 Sv. Even though the tidal velocity is rather large, occasionally higher than 10 cm/s, the transport correction was nevertheless only 20%. The reason is that the larger corrections are essentially in the shallower water regions with a small contribution to the imbalance. Further corrections were made to implement the inverse model (described below).

Figure 9 shows the average velocity and integrated velocity using LADCP data after detiding. In the average velocity plot, currents are 10–30 cm/s near the slope and shelf break in both the southern and northern

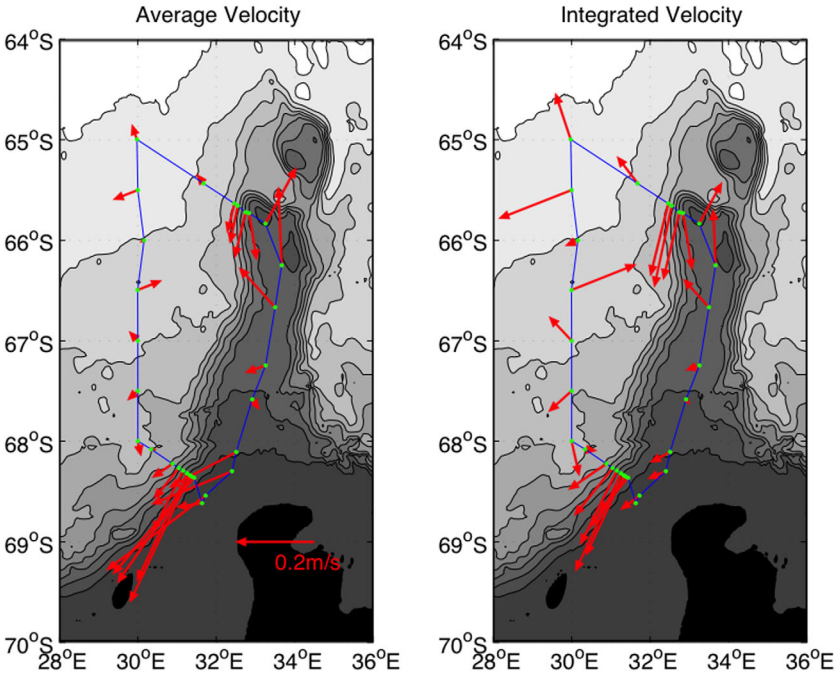

Figure 9. Vertical average detided velocities (left) and integrated velocity (right; relative transport contribution) from the Lowered ADCP data.

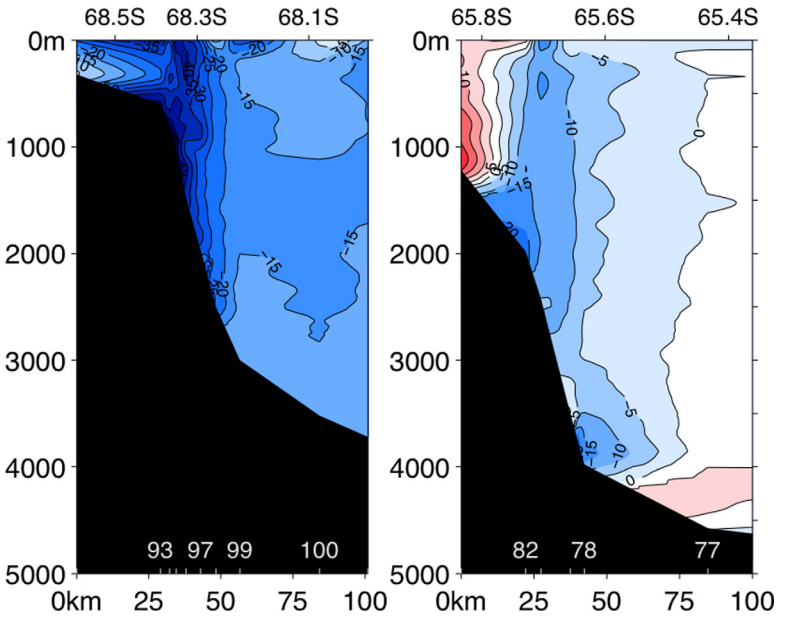

Figure 10. The detided LADCP meridional (approximately along-isobath component) velocities (cm/s) of the southern/western section (left) and northern section (right). Blue is southward, red is northward.

part of the bank; maximum speeds were up to 50 cm/s. The ASC in the box region splits into two parts due to the topography. The upper part of the ASC, which is shallower than 1000 m, can flow over the bank near the coast; the lower part, which is on the slope deeper than 1000 m, has to go around the bank following the isobaths. Near the northern tip of the bank, the flow is up to 20 cm/s and some reversals were observed, indicating possibly a recirculation around local topographic highs. Depth-integrated velocity on the slope at both sections is comparable, suggesting that most of the water rounds the outer tip of the bank.

To show the vertical structure of the ASC on the slope, the detided meridional LADCP velocities on north and south section are shown in Figure 10. Southward flow on both sections with a dominantly barotropic structure is present. The maximum flow is from water depths of 500–2000 m on the southern slope and from 1000 to 3000 m on the northern slope. In addition, at the bottom of the northern slope, there is a bottom intensified flow below 3500 m depth, associated with CFC anomalies. This is the more recently formed dense water flowing into the Weddell Gyre.

To obtain the total velocity at station pairs for box-inversion purposes, the geostrophic velocity from the thermal wind is referenced to the LADCP data. First, the LADCP profiles are compared to the geostrophic velocity from the CTD data to select the depth range in which the two shears match; then the two mean velocities in this range are matched. Generally, the middle one-third of the profile is picked as reference. After this step, the box transport imbalance discussed below is reduced to 3 Sv. Without this step, it is not possible to find a consistent solution using the inverse method, since the initial transport is too far from a mass-balancing solution.

4.2. Inverse Model

Since our observations formed a boxed region, it is convenient to use an inverse method to combine the LADCP data, CTD data, and the thermal wind relation to get a statistically consistent estimate of the transport. In our box, the water column is divided into 13 layers by 12 neutral density surfaces (Table 1). Following *Joyce et al*. [1986], the model equation for each layer is

$$\sum a_{p,j}v_j + a'_{p,i}w_i + a'_{p,i-1}w_{i-1} + n = 0;\ \ i = 1,\ldots,12;\quad j = 1,\ldots,\ 29;\ \ p = 1,\ \ 2,\ \ 3 \tag{1}$$

where the p refers to the pth conservation statement, j to station pair, and i to layer interface; the coefficients, a, a' are the appropriate property concentration times the corresponding boundary area; and n is the noise. The constraints are chosen as: (a) Total mass and the mass in each layer is conserved; (b) Salt in each layer is conserved, except for the upper two layers; and (c) Heat in each layer is conserved, except for

Table 1. Neutral Density (kg/m^3) of Box-Model Interfaces, and Approximate Average Depth (m)

1	27.90	100
2	28.03	250
3	28.08	450
4	28.13	700
5	28.17	800
6	28.21	1200
7	28.24	1700
8	28.27	2100
9	28.30	2600
10	28.32	3000
11	28.34	3500
12	28.36	4000

the upper two layers, which intersect the upper part of the bank. If we include the first two layers for conservation of heat and mass, we cannot achieve a balanced inverse solution, probably due to time-dependent sampling issues and the strong air-sea-ice interaction for these two layers. The transport uncertainty for each layer is chosen as 0.3 Sv and as 0.1 Sv for total flow, following *Joyce et al.* [1986].

The absolute velocity for each layer, v_j, is sum of the reference velocity, v_j^b, and the thermal wind velocity, v_j', as in equation

$$v_j = v_j^b + v_j' \quad j = 1,\ 29 \tag{2}$$

Since we know the prior reference velocities, v_j^b, at 29 station pairs from the LADCP data, b_j, we can add another 29 constraints.

$$v_j^b = b_j + n \quad j = 1,\ 29 \tag{3}$$

In total, we have 41 unknowns and 65 equations. The solution is found by Gauss-Markov estimation. The reference velocities, v^b, are estimated and the effective diapycnal velocities, w, are estimated as well.

Using the estimated velocities, the cumulative transport is calculated along the box clockwise starting from the northwest corner (Figure 11). The maximum transport reaches 13 Sv at the southernmost station 92. The transport on the north section splits into two currents: one on the shallower slope and one on the deeper slope. Near the continental break, a recirculation has a transport approaching 10 Sv. On the primary I6S section (the southern or western section), the two flows converge. The transport of the ASC from the coast to the 3500 m isobath is 9.6 $\pm$ 2.3 Sv (Stations 77–92 and 92–100). The transport associated with the northern section's outer slope front is about 4.0 $\pm$ 0.3 Sv, of which 1.8 $\pm$ 0.3 Sv goes into the Weddell Gyre as newly formed Weddell Sea Deep Water. This transport of newly formed inflow into the Weddell Gyre is comparable to the estimate of 2.0 $\pm$ 0.4 Sv by *Schodlok et al.* [2001], and consistent with the gyre inflow estimated by *Jullion et al.* [2014].

The effective diapycnal transport extracted from the inverse model is shown in Figure 12. The maximum upward transport of 0.5 Sv is at a neutral density of 28.27 kg/m^3, which is the maximum density in the Weddell Deep Water density class. About 1.3 Sv converges at intermediate densities into the 28.22 kg/m^3 density layer. This indicates that lighter water and denser water mix together to form intermediate-density water. The depth of the 28.22 kg/m^3 density level intersects the bank near 1000 m depth, suggesting a vertical circulation scheme in which the water flowing from east to west near the break in the slope on the bank mixes, modifying the CDW mass on the bank and transferring it to greater density. The magnitude of this diapycnal transport is estimated at about 1.3 Sv, which is significant relative to the total horizontal

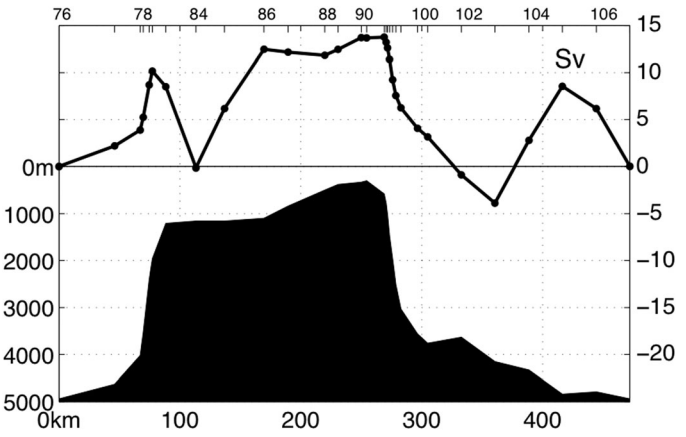

Figure 11. Cumulative transport along the box versus distance (upper curve), with station depth (solid black). The station numbering begins at the northwest corner of the box, and continues clockwise. The reference velocities are adjusted by the inverse model to reduce the net imbalance to below 1 Sv.

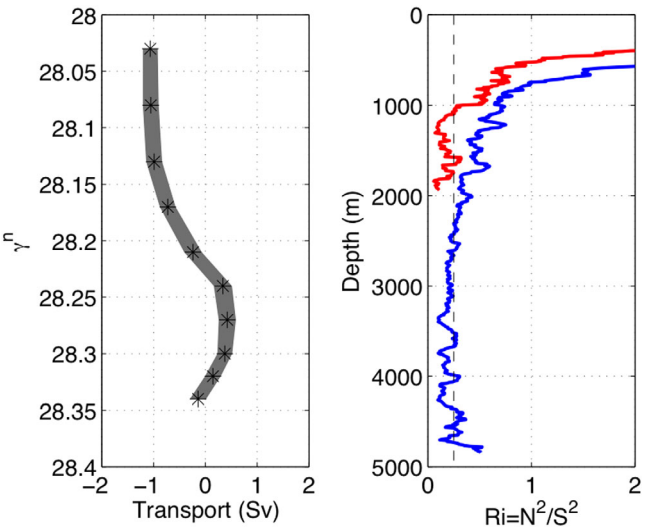

Figure 12. (left) Diapycnal volume transport in the box; shading is standard error. Positive values are toward decreasing neutral density (top). (right) The average Richardson-number: the red line is the average of stations shallower than 2000 m; the blue line is the average of stations deeper than 2000 m; the vertical line is Ri = 0.25. Refer to Figure 5 for depth of neutral density.

transport. This would translate into an average mixing coefficient of about 3×10^{-3} m^2s^{-1}, which is high, but not unlike values above seamounts [e.g., *Kunze and Toole*, 1997].

5. Summary and Discussion

CLIVAR I6S cruise observations are used to study the Antarctic Slope Current near 30°E in the eastern boundary region of the Weddell Gyre. A horizontal and vertical current circulation scheme is presented in Figure 13, showing the ASC split into two branches: a shallow one which can flow directly over the Gunnerus Bank and a branch extending to depths greater than 1000 m, which flows around the bank. Evidence for a deep eddy in the main I6S section just north of the bank with properties consistent with an upstream source [*Speer et al*., 2009] suggests that such eddies may carry water in the Slope Current offshore and mix properties along isopycnals between the interior and the slope region due to the topographic disturbance to the flow.

An inverse method is used to estimate the transport associated with the ASF and Slope Current, at 9.6 ± 2.3 Sv. About 2 Sv are associated with the inner front on the bank, or Coastal Current, and an additional 4 Sv are associated with the outer slope front beyond the 3500 m isobath north of the bank.

Klatt et al. [2005] estimated the ASC transport at the prime meridian as 26 Sv, but this transport estimate includes the transport down to 5000 m depth. *Heywood et al*. [2000] estimated the total ASF transport as 14 Sv along longitude 9°W, to depths of 4000 m. If we account for all the transport on the slope shallower than

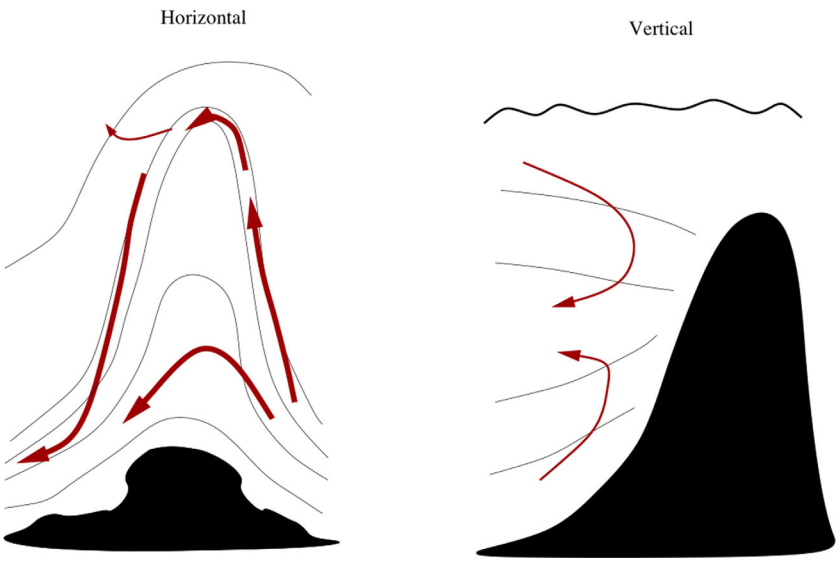

Figure 13. Schematic of the horizontal and vertical circulation near the Gunnerus Bank region. (right) Horizontal circulation shows flow from farther east riding up onto the bank, some of which follows a shallow path while the rest flows around the bank along the slope. The vertical circulation schematically shows the convergence of water at intermediate depths due to mixing on the bank.

3000 m depth, the transport is close to 12 Sv. These several transport estimates are comparable if we consider only the Slope Current component of transport, down to depths of 3000–4000 m.

Two distinct mixing mechanisms within the Slope Current appear to be operating near the Gunnerus Bank: a small-scale diapycnal mixing on the bank itself, and a deeper, mesoscale, lateral mixing flow rounding the bank where eddies are shed to the interior. Richardson-number was calculated to investigate further (Figure 12). Below the surface layer, the Richardson-number is relatively small largely due to weak stratification, and consistent with stronger small-scale mixing. To distinguish the possible role of the bank on mixing, we also calculated the Richardson-number for stations shallower 2000 m and deeper 2000 m separately. The Richardson-number of shallow stations is smaller than those of the deep stations, especially between 1000 and 2000 m depth, due mainly to the larger shear over the bank. Upslope and downslope advection in the bottom Ekman layer flow may be playing a role in the diapycnal circulation on the bank as well.

Nøst et al. [2011] have suggested that eddy processes, together with Ekman transports, control the cross-slope movement of warm deep water along the bottom in the eastern Weddell Sea. They discuss the role of the net input of buoyancy by ice melt and its consistency with residual overturning due to eddies. For the buoyancy input (at lower density) to exert such control on the inflow mixing must be occurring as well, but this mixing does not have to be at the same location as the eddy fluxes. The Gunnerus Bank may be a location where both eddy and mixing effects are enhanced.

Acknowledgments
Hydrographic data from the I6S line is publicly available at the CCHDO http://cchdo.ucsd.edu/. The abilities of the Captain and crew of the R/V Revelle enhanced the scientific return in this remote region and the hard work of the 2008 I6S sampling groups is appreciated. This work was supported by NSF grants OCE-0927583, OCE-0622670 and OCE-1231803.

References

Archambeau, A.-S., C. Pierre, A. Poisson, and B. Schauer (1998), Distributions of oxygen and carbon stable isotopes and CFC-12 in the water masses of the Southern Ocean at 30E from South Africa to Antarctica: Results of the CIVA1 cruise, *J. Mar. Syst.*, *17*, 25–38.

Carmack, E. (1974), Quantitative characterization of water masses in Weddell Sea during summer, *Deep Sea Res. Oceanogr. Abstr.*, *21*(6), 431–443.

Chavanne, C. P., K. J. Heywood, K. W. Nicholls, and I. Fer (2010), Observations of the Antarctic Slope Undercurrent in the southeastern Weddell Sea, *Geophys. Res. Lett.*, *37*, L13601, doi:10.1029/2010GL043603.

Couldrey, M. P., L. Jullion, A. C. Naveira Garabato, C. Rye, L. Herráiz-Borreguero, P. J. Brown, M. P. Meredith, and K. L. Speer (2013), Remotely induced warming of Antarctic Bottom Water in the eastern Weddell gyre, *Geophys. Res. Lett.*, *40*, 2755–2760, doi:10.1002/grl.50526.

Fahrbach E., G. Rohardt, and G. Krause (1992), The Antarctic Coastal Current in the southeastern Weddell Sea, *Polar Biol.*, *12*, 171–182.

Gill, A. (1973), Circulation and bottom water production in Weddell Sea, *Deep Sea Res. Oceanogr. Abstr.*, *20*(2), 111–140.

Hellmer, H. H., F. Kauker, R. Timmermann, J. Determann, and J. Rae (2012), Twenty-first-century warming of a large Antarctic ice-shelf cavity by a redirected coastal current, *Nature*, *485*(7397), 225–228.

Heywood, K. J., R. A. Locarnini, D. Russell, P. F. D. Frew, and B. A. King (2000), Transport and water masses of the Antarctic Slope Front system in the eastern Weddell Sea, in, *Ocean, Ice, and Atmosphere: Interactions at The Antarctic Continental Margin, Antarct. Res. Ser.*, vol. 75, edited by S. S. Jacobs, and R. F. Weiss, pp. 203–214, AGU, Washington, D. C.

Hoppema, M., O. Klatt, W. Roether, E. Fahrbach, K. Bulsiewicz, C. Rodehacke, and G. Rohardt (2001), Prominent renewal of Weddell Sea deep Water from a remote source, *J. Mar. Res.*, *59*(2), 257–279.

Joyce, T., C. Wunsch, and, S. Pierce (1986), Synoptic Gulf Stream velocity profiles through simultaneous inversion of hydrographic and acoustic Doppler data, *J. Geophys. Res.*, *91*(C6), 7573–7585.

Jullion, L., et al. (2014), The contribution of the Weddell Gyre to the lower limb of the Global Overturning Circulation, *J. Geophys. Res. Oceans*, *119*, 3357–3377, doi:10.1002/2013JC009725.

Klatt, O., E. Fahrbach, M. Hoppema, and G. Rohardt (2005), The transport of the Weddell Gyre across the Prime Meridian, *Deep Sea Res., Part II*, *52*(3–4), 513–528.

Kunze, E., and J. M. Toole (1997) Tidally driven vorticity, diurnal shear, and turbulence atop fieberling seamount, *J. Phys. Oceanogr.*, *27*, 2663–2693.

Meredith, M., R. Locarnini, K. Van Scoy, A. Watson, K. Heywood, and B. King (2000), On the sources of Weddell Gyre Antarctic Bottom Water, *J. Geophys. Res.*, *105*(C1), 1093–1104.

Nøst, O. A., M. Biuw, V. Tverberg, C. Lydersen, T. Hattermann, Q. Zhou, L. H. Smedsrud, and K. M. Kovacs (2011) Eddy overturning of the Antarctic Slope Front controls glacial melting in the Eastern Weddell Sea, *J. Geophys. Res.*, *116*, C11014, doi:10.1029/2011JC006965.

Orsi, A. H., T. Whitworth III, and W. D. Nowlin Jr. (1995), On the meridional extent and fronts of the Antarctic Circumpolar Current, *Deep Sea Res., Part I*, *42*, 641–673.

Park, Y., E. Charriaud, P. Craneguy, and A. Kartavtseff (2001), Fronts, transport, and Weddell Gyre at 30E between Africa and Antarctica, *J. Geophys. Res.*, *106*(C2), 2857–2879.

Schodlok, M., C. Rodehacke, H. Hellmer, and A. Beckmann (2001), On the origin of the deep CFC maximum in the eastern Weddell Sea: Numerical model results, *Geophys. Res. Lett.*, *28*(14), 2859–2862.

Schroder, M., and E. Fahrbach (1999), On the structure and the transport of the eastern Weddell Gyre, *Deep Sea Res., Part II*, *46*(1–2), 501–527.

Speer, K. G., T. Dittmar, and J. Swift (2009), CLIVAR I6S cruise report, Scripps Institute of Oceanography, San Diego, Calif.

Thurnherr, A. M. (2012), The finescale response of lowered ADCP velocity measurements processed with different methods, *J. Atmos. Oceanic Technol.*, *29*, 597–600.

Whitworth, I., A. H. Orsi, S. -J. Kim, and W. D. Nowlin (1998), Water masses and mixing near the Antarctic Slope Front, in *Ocean, Ice, and Atmosphere: Interactions at the Antarctic Continental Margin, Antarct. Res. Ser.*, vol. 75, edited by S. S. Jacobs and R. F. Weiss, pp. 1–27, AGU, Washington, D. C.